Journal of Drug Delivery Science and Technology 124 (2026) 108613

Contents lists available at ScienceDirect

Journal of Drug Delivery Science and Technology

journal homepage: www.elsevier.com/locate/jddst

# Dissecting the barriers to PDMAEMA-mediated gene delivery: molecular weight drives efficiency while endosomal escape limits potential

Flaminia Fruzzetti [1], Ilaria Porello [1], Nina Bono, Francesco Cellesi [*], Gabriele Candiani [**]

*Dept. of Chemistry, Materials and Chemical Engineering "Giulio Natta", Politecnico di Milano, Via Bassini 6, Milan, 20133, Italy*

ARTICLE INFO

*Keywords:*
Gene delivery
PDMAEMA
Transfection
Non-viral vectors
Endosomal escape

ABSTRACT

Efficient intracellular delivery remains a major bottleneck in nucleic acid–based therapeutics. Among non-viral vectors, poly(2-(dimethylamino)ethyl methacrylate) (PDMAEMA) offers tunable cationic properties and synthetic versatility, yet its limited endosomal escape capacity constrains transfection efficiency (TE). In this work, PDMAEMA-based polyplexes were systematically investigated to elucidate how molecular weight (MW), macromolecular architecture (linear vs. star-shaped), and hydrophobic modification with poly(ε-caprolactone) (PCL) influence gene delivery performance. To this end, a library of cationic polymers was synthesized via Atom Transfer Radical Polymerization (ATRP) and characterized in terms of DNA condensation ability, polyplex physicochemical properties, cytotoxicity (CT), and TE. Linear PDMAEMA (L-PDMAEMA) in the medium- and high-MW ranges (10-20 kDa) provided the optimal balance between charge density and colloidal stability, achieving TE comparable to the benchmark 25 kDa branched polyethyleneimine (*b*PEI) while exhibiting significantly lower CT. Conversely, star-shaped and micellar architectures exhibited reduced TE, likely due to steric hindrance affecting charge accessibility. To overcome endosomal entrapment, chloroquine (CQ) was employed as an endosomal escape enhancer, resulting in up to a 30-fold increase in TE for L-PDMAEMA without measurably affecting cell viability. Overall, this study demonstrates that rational tuning of polymer topology and MW enables PDMAEMA-based vectors to combine high TE with minimal CT, emphasizing the potential of integrating intrinsic endosomal escape functionality in future polymer designs.

## 1. Introduction

The clinical success of nucleic acid (NA)-based therapeutics critically depends on the safe and efficient intracellular delivery of genetic cargo [1–3].

Naked NAs are rapidly degraded and poorly internalized, necessitating delivery vectors to mediate efficient cellular uptake [2].

Vector-mediated gene delivery, particularly using non-viral vectors, has attracted increasing attention as a safer and more adaptable alternative to viral counterparts [2,4–7]. Non-viral carriers mainly include cationic polymers (CPs), which form nanocomplexes (polyplexes) through electrostatic interactions established between their positive charges and negatively charged NAs. These polyplexes offer several advantages, including improved stability, reduced immunogenicity, tunable chemistry, and scalable production [8].

Despite these advantages, non-viral carriers face significant limitations related to transfection efficiency (TE), which reflects the overall capacity of a vector to mediate functional transgene expression in target cells. This latter aspect critically depends on endosomal escape mechanisms [9,10]. CPs often exploit the "proton sponge effect", whereby buffering amine groups induce endosomal swelling and rupture, thereby releasing NAs into the cytosol [11]. However, this mechanism is often insufficient, prompting the development of complementary strategies including the use of fusogenic or pore-forming peptides that destabilize endosomal membranes, ionizable lipids that trigger membrane fusion, and stimuli-responsive systems (e.g., light, ultrasound, or magnetic fields) that mechanically or chemically disrupt vesicles [12–16].

Among CPs, polyethyleneimine (PEI) has long served as a benchmark for transfection studies due to its high efficiency, particularly the 25 kDa branched variant (*b*PEI) [17]. In recent years, attention has also focused

* Corresponding author.
** Corresponding author.
*E-mail addresses:* francesco.cellesi@polimi.it (F. Cellesi), gabriele.candiani@polimi.it (G. Candiani).
[1] Authors contributed equally to this work.

https://doi.org/10.1016/j.jddst.2026.108613
Received 17 April 2026; Received in revised form 9 June 2026; Accepted 16 June 2026
Available online 16 June 2026

on poly(2-(dimethylamino)ethyl methacrylate) (PDMAEMA), a synthetic polymer with tertiary amino groups that protonate at physiological pH, thus enabling NA condensation [18,19]. PDMAEMA is a versatile polymer that can be synthesized with varying molecular weights (MWs) and architectures (linear, branched, and star-shaped) using controlled/living polymerization techniques such as atom transfer radical polymerization (ATRP) and reversible addition-fragmentation chain transfer (RAFT) [20–23]. Studies indicate that high-MW (HMW) PDMAEMA offers superior TE, although often at the expense of increased cytotoxicity (CT). Branched architectures can partially mitigate this by shielding cationic groups within the three-dimensional polymer framework, reducing nonspecific membrane interactions while maintaining polyplex stability [24].

Despite these advantages, PDMAEMA exhibits limited ability to disrupt endosomal membranes, which hampers the TE of the resulting polyplexes [25]. Recent findings suggest that PDMAEMA only induces morphological changes in endosomes rather than physical rupture [23]. Therefore, enhancing TE may require co-treatment with endosome-disrupting agents to facilitate endosomal release [26,27]. Among these agents, chloroquine (CQ) has been well-documented for its ability to induce endosomal membrane destabilization [26,28], though its potential to enhance PDMAEMA-based systems remains underexplored [29,30].

This study investigates the performance of PDMAEMA-based polyplexes for gene delivery through a systematic structure–activity relationship (SAR) approach. To this end, we synthesized a library of PDMAEMA polymers with varying MWs and architectures (linear and branched), examining how these structural variations influence CT and TE. Particular attention is devoted to low-MW (LMW) PDMAEMA, for which performance data remain scarce and inconclusive [31,32]. To evaluate the effect of amphiphilic balance on key physicochemical properties, block copolymers composed of PDMAEMA and the hydrophobic polyester poly(ε-caprolactone) (PCL) were also investigated. The PCL incorporation was intended to modulate the amphiphilic balance, potentially promoting self-assembly into stable nanostructures and enhancing membrane interactions, although excessive hydrophobicity can compromise solubility and increase CT.

A central aim of this work is therefore to establish SARs linking polymer structural features to endosomal escape efficiency and, ultimately, to transfection performance, using CQ as a diagnostic tool to dissect the contribution of endosomal entrapment.

## 2. Materials and methods

### 2.1. Materials and reagents

HeLa (human cervical adenocarcinoma cells, CCL-2) cell line was purchased from the American Type Culture Collection (ATCC, Manassas, VA, USA). Alamar Blue® cell viability assay was purchased from Life Technologies Italia (Monza, Italy). Bicinchoninic acid (BCA) Protein Assay Kit was purchased from Pierce Chemical (Rockford, IL, USA). pGL3 (pDNA encoding the modified Firefly luciferase, pGL3-Control Vector, 5.256 kbp) and Luciferase Assay System were obtained from Promega (Milan, Italy). Dimethyl Sulfoxyde-$d_6$ 100 % (DMSO-$d_6$) was purchased from Eurisotop (Molsheim, France).

All the following reagents were purchased from Merck Life Science (Milan, Italy): salmon sperm DNA (~50-100 kDa, corresponding to ~ 77-154 bp); 200× SYBR Green I; Trypan Blue Solution 0.4 % (liquid, sterile-filtered, suitable for cell culture); Dulbecco's Phosphate Buffered Saline (PBS); Dulbecco's Modified Eagle Medium (DMEM) supplemented with 1 mM sodium pyruvate, 10 mM 4-(2-hydroxyethyl)-1-piperazineethanesulfonic acid sodium salt (HEPES) buffer, 100 U/mL penicillin, 0.1 mg/mL streptomycin, 2 mM glutamine and 10 % (v/v) fetal bovine serum (FBS) (hereafter referred to as complete Medium, cDMEM); trypsin-EDTA solution 1 × (sterile-filtered, BioReagent, suitable for cell culture, 5.0 g porcine trypsin and 2 g EDTA × 4 Na per liter of 0.9 % sodium chloride, NaCl); PDMAEMA - average $M_n$ 10,000 Da (hereafter referred to as 10 kDa L-PDMAEMA), #909866; NaCl; ε-caprolactone 97 % (ε-CL); (dimethylamino)ethyl methacrylate ≥98 % (DMAEMA); benzyl alcohol 99.8 % anhydrous (BnOH); RhodamineB ≥95 % (RhB); α-bromoisobutyryl bromide 98 % (BiBB); ethyl-α-bromoisobutyrate 98 % (EBiB); pentaerythritol tetrakis(2-bromoisobutyrate) ≥ 99 % (PET–BIB); 2,2′-bipyridyl ≥99 % (BPY); Tin (II) 2-ethylhexanoate 92-100 % ($Sn(Oct)_2$); Copper (I) bromide 98 % (CuBr(I)); methanol ≥99.8 % (MeOH); tetrahydrofuran ≥99.9 % anhydrous inhibitor-free (THF); tetrahydrofuran ≥99.9 % gel permeation chromatography grade (THF); toluene ≥99.9 % anhydrous; dichloromethane ≥99.8 % (DCM); triethylamine ≥99 % (TEA); hexane ≥99 %; deuterochloroform ≥99.8 % ($CDCl_3$); aluminum oxide ($Al_2O_3$); sodium bicarbonate ($NaHCO_3$); sodium sulphate ≥99 % ($Na_2SO_4$). All chemicals were used without further purification unless otherwise indicated.

### 2.2. Polymers synthesis and characterization

#### 2.2.1. Polymers characterization

Monomer conversion ($\chi_{ROP}$, $\chi_{ATRP}$) and polymer degree of polymerization (DP) were determined by $^1$H NMR analysis, dissolving crude and purified polymers in the proper deuterated solvent. $^1$H NMR spectra were recorded on a Bruker Avance 400 MHz spectrometer at 298 K, using $CDCl_3$ or DMSO-$d_6$ as solvent. Chemical shifts ($\delta$) are reported in ppm downfield from the deuterated solvent used as the internal standard.

The polymers number-average molar mass ($M_{n,SEC}$) and dispersity (Đ) values were evaluated using a Jasco® LC-2000Plus size exclusion chromatography (SEC) instrument equipped with a refractive index detector (RI-2031Plus, Jasco), a CO-2060 plus oven column, and a PU-2080 pump, 3× Agilent PLgel columns (300 × 7.5 mm, particle size Ø = 5 μm) and 1× PLgel guard (50 × 7.5 mm, particle size Ø = 5 μm) using THF as eluent at 35 °C. The instrument was calibrated by using polystyrene standards (calibration kits by RESTEK and Sigma-Fluka). Samples of purified polymer were dissolved in THF (containing 250 ppm BHT as inhibitor) at 4 mg/mL, filtered through PTFE syringe filters (Ø = 0.22 μm) and injected at a flow rate of 1 mL/min, using a Jasco AS-2055Plus autosampler.

#### 2.2.2. Potentiometric acid-base titration

The apparent pKa of each polymer was determined by potentiometric acid-base titration. Polymers were dissolved at 10 mM amine concentration in deionized water ($dH_2O$) and acidified to pH ≈ 3 by dropwise addition of 1 M HCl. Back-titration was performed by adding 0.01 M NaOH in small increments under a nitrogen atmosphere at 25 °C, recording the pH after each addition until a stable value was reached. The apparent pKa was extracted using the half-equivalence point method: the volume at which free HCl was fully neutralised ($V_{HCl}$, identified as the first maximum of the first derivative ΔpH/ΔV) and the amine equivalence-point volume ($V_{eq}$, identified as the largest maximum of the first derivative ΔpH/ΔV) were determined for each polymer. The same rule was applied identically to all the polymers tested, and the residual free-acid volume was cross-checked against the free-acid content estimated from the initial pH. The apparent pKa was defined as the pH value read from the titration curve at $V_{half}$ [33], defined in eq. (1):

$$V_{half} = \frac{(V_{HCl} + V_{eq})}{2} \quad (1)$$

#### 2.2.3. Synthesis of $PCL_n$-Br macroinitiator

The reported procedure is adapted from previous works [1,8,34]. The monomer (m) ε-caprolactone (5 g, 43.8 mmol) was inserted in a round double-neck flask, and three cycles of nitrogen/vacuum of 5 min each were performed. The initiator (I) BnOH (eq. m/eq. I = n, where n = 30) and the catalyst (C) $Sn(Oct)_2$ (eq. C/eq. I = 0.1) were then

added, maintaining the system under nitrogen flow. The mixture was stirred overnight at 130 °C. The reaction was stopped by cooling the flask to room temperature (r.t.). Purification was carried out by dissolving the crude in DCM (2.5 g/mL) and dropping it into cold MeOH (MeOH/DCM = 100/1 (v/v)). The system was kept under vigorous stirring in an ice bath throughout the precipitation process. The resulting precipitate was isolated from the supernatant through filtration, and the filtrate was dried under reduced pressure at 50 °C, obtaining the final product as a white powder. Yield >90 %. Conversion $\chi$ = 99 % (from $^1$H NMR data).

For the functionalization of $PCL_n$ with bromine moieties, 5 g of $PCL_n$ (1 eq.) were added in a double-neck flask, evacuated and backfilled with nitrogen three times, then dissolved in 6 mL of dry toluene, and cooled at 0 °C in an ice bath. TEA (1.7 eq.) and BiBB (1.5 eq.) were dissolved in 1 mL of toluene each and stirred for 10 min. TEA and BiBB solutions were added dropwise to the reaction mixture through a dropping funnel. The reaction mixture was then brought back to r.t. and stirred overnight at 60 °C in an oil bath. The resulting solution was dried under reduced pressure until toluene was completely evaporated, and the crude product was dissolved in 5 mL of DCM. An aqueous solution ($\varphi_{acq}$) of $NaHCO_3$ at pH ≥ 8 was prepared by dissolving ~ 3 g of salt in 60 mL of water. The polymer solution ($\varphi_{org}$) obtained after the filtration was inserted in a separating funnel and washed three times with the $NaHCO_3$ solution ($\varphi_{org}/\varphi_{acq}$ ~ 1/1 (v/v) for each wash) to extract the desired product in the organic phase. The water phase collected at the end of the washing steps was mixed with additional DCM ($\varphi_{org}/\varphi_{acq}$ ~ 1/1 (v/v)) for the complete recovery of the product. Anhydrous $Na_2SO_4$ was added to the organic solution for water adsorption, with consequent salt removal through filtration. The filtrate was dried under reduced pressure, then dissolved in 2 mL of DCM and dropped into 250 mL of cold MeOH, maintaining the system under stirring in an ice bath. The solution was then filtered to isolate the precipitate, obtaining the final product as a slightly yellow viscous oil. Yield >90 %. $^1$H NMR (400 MHz, $CDCl_3$), $\delta$ (ppm): $\delta$ 7.34 (m, 5H, $C_6H_5$- $CH_2$-), 5.11 (s, 2H, $C_6H_5$-$CH_2$-OC(O)-), 4.06-4.05 (t, 2H·*n*, -$CH_2$-OC(O)-), 2.30 (t, 2H·*n*, –OC(O)–$CH_2$-), 1.93–1.92 (s, 6H, -$C(CH_3)_2$-Br), 1.65 (m, 4H·*n*, -OC(O)-$CH_2CH_2$-, -$CH_2CH_2$-OC(O)-), 1.38 (m, 2H·*n*, -$CH_2CH_2CH_2$-), where *n* is PCL degree of polymerization.

#### 2.2.4. PDMAEMA polymers synthesis

MeOH or THF were degassed under nitrogen atmosphere for 30 min before use. The reaction initiator (I, 1 eq.), and the monomer DMAEMA were introduced into a Schlenk flask, followed by three consecutive nitrogen/vacuum cycles (5 min each). For the synthesis of $PDMAEMA_m$ (linear $PDMAEMA_m$) homopolymers, EBiB was employed as the initiator, whereas the amphiphilic block copolymers $PCL_n$-b-$PDMAEMA_m$ were prepared using $PCL_n$-Br as macroinitiator. The monomer-to-initiator ratio (DMAEMA/I = m) was adjusted according to the targeted degree of polymerization (DP = m). Four-arm (4A) branched PDMAEMA polymers were synthesized analogously using PET–BIB (1 eq.) as the initiator. In this case, the monomer feed was calculated to achieve the desired overall degree of polymerization (DMAEMA/I = 4 × m, where m corresponds to the target DP per arm).

The catalyst solution (C) was prepared separately by inserting CuBr (574 mg) and BPY (864 mg) in a double-necked flask, followed by three nitrogen/vacuum cycles. Degassed MeOH (2 mL) was then added, and the mixture was stirred at r.t. under nitrogen for 10 min to obtain a homogeneous catalyst complex. The polymerization mixture was subsequently prepared by dissolving the monomer and initiator in MeOH ([DMAEMA] ≤ 1 M) in case of EBIB or PET-BIB initiators, or THF in case of $PCL_n$-Br macroinitiator, heating up to 50 °C to ensure complete dissolution. The catalyst solution was then introduced ([C]/[L]/[I] = 1/2/1), and the reaction mixture was allowed to polymerize overnight at 30 °C.

The crude product was purified by filtration through a short silica pad (h = 3 cm, Ø = 2 cm), eluting with DCM. The filtrate was concentrated under reduced pressure up to a concentration of 2 mg/mL. The polymer solution was then precipitated dropwise into cold hexane (DCM/hexane = 1/100 (v/v)) under stirring in an ice bath. The suspension was stored at −20 °C for 30 min, and the precipitated polymer was collected by filtration. Fluorescently labeled analogs were synthesized following the same procedure, incorporating HEMA–RhB as a comonomer (molar ratio HEMA–RhB:DMAEMA = 1:100). This approach yielded fluorescent polymers with identical structural and compositional design parameters to their non-labeled counterparts. Yield >80 %.

$PDMAEMA_m$ - $^1$H NMR (400 MHz, $CDCl_3$), $\delta$ (ppm): $\delta$ 4.10 (s, 2H·*m*, O-$CH_2$-), 2.7 (s, 2H·*m*, -$CH_2$-N-), 2.35 (s, 6H·*m*, -$N(CH_3)_2$), 1.60–2.00 (m, 2H, $CH_{2,backbone}$), 1.95 (s, 6H, -$CH_2OC(O)C(CH_3)_2$-), 1.2-0.6 (m, 3H·*m*, $CH_{3,backbone}$) where *m* is PDMAEMA degree of polymerization.

$PCL_n$-$PDMAEMA_m$ - $^1$H NMR (400 MHz, $CDCl_3$), $\delta$ (ppm): $\delta$ 7.34 (s, 5H, PCL: $C_6H_5$-$CH_2$-), 5.11 (s, 2H, PCL: $C_6H_5$-$CH_2$-OC(O)-), 4.14-4.02 (m, 2H·*n* + 2H·*m*, PCL: -$CH_2$-OC(O)-, PDMAEMA: -O-$CH_2$-), 3.10-2.30 (m, 2H·*m*, PDMAEMA: -$OCH_2CH_2N$-), 2.32-2.25 (t, 2H·*n*, PCL: -OC(O)-$CH_2$-), 2.60-2.20 (s, 6H·*m*, PDMAEMA: -$N(CH_3)_2$), 1.92 (s, 6H, -$CH_2OC(O)C(CH_3)_2$-), 1.48-1.65 (m, 4H·*n*, PCL: -OC(O)-$CH_2CH_2$-, -$CH_2CH_2$-OC(O)-), 1.25-1.38 (m, 2H·*n*, PCL: -$CH_2CH_2CH_2$-), 1.2-0.6 (m, 3H·*m*, PDMAEMA: $CH_{3,backbone}$), where *n* is PCL degree of polymerization, *m* is PDMAEMA degree of polymerization.

### 2.3. PCL-PDMAEMA nanoparticles formulation

PCL-PDMAEMA micelles were prepared according to a nanoprecipitation/solvent evaporation method [8,33]. Briefly, 5 mg of copolymer were dissolved under stirring in 1 mL of acetone. The solution was added dropwise into 1 mL of $dH_2O$ and stirred for 10 min. Acetone was removed at the rotary evaporator under controlled pressure gradient (from 1000 mbar to 100 mbar in 1 h, and then setting it at 100 mbar for 1 h) at 30 °C. Particle size distribution, average size (expressed as hydrodynamic diameter, $D_H$), polydispersity index (PdI), and surface charge (expressed as zeta potential, $\zeta_P$) were evaluated at 25 °C through Dynamic Light Scattering (DLS) and Electrophoretic Light Scattering (ELS) using a Malvern Zetasizer Nano ZS instrument (Malvern, UK) equipped with a 4 mW He−Ne laser operating at $\lambda$ = 632 nm (backscattered angle 173°).

### 2.4. Preparation of polymer solutions

All PDMAEMA polymers in their dried form were initially dissolved in $dH_2O$. PCL-PDMAEMA micellar suspension was diluted with $dH_2O$ up to the final desired concentration. All solutions were prepared with a polymer concentration corresponding to 10 mM of total amine ([N]). The number of moles of amines was theoretically calculated based on the polymer's $M_n$ and its DP. The pH of all solutions was adjusted to 7-7.5 by adding 0.1 M HCl or 0.1 M NaOH. Aliquots of the polymer solutions were stored at 4 °C until use.

### 2.5. Preparation of PDMAEMA/DNA complexes

Before complexation, polymer and pDNA stock solutions were warmed to r.t. Polyplexes were prepared by adding the 0.25 μg/μL aqueous solution of pDNA to polymer solutions, formulated at the desired concentration to yield different N/Ps (i.e., 5, 10, 15, 20, 25, 30, and 40), where N/P is defined as the number of amines (N) of the polymer used to complex the phosphate groups (P) of a given amount of NA. Afterward, polyplexes were incubated for 20 min at r.t.

### 2.6. Evaluation of DNA binding

The DNA-binding ability of PDMAEMA polymers was evaluated using a fluorophore displacement assay, as reported elsewhere [34]. Briefly, polymer solutions and double-stranded salmon sperm DNA were pre-warmed to r.t. and vortexed for 10 s. Polyplexes were prepared by

mixing the polymer solution with a solution of DNA (0.5 mg/mL) containing the intercalating fluorophore SYBR Green I (200×, $\lambda_{ex} = 497$ nm, $\lambda_{em} = 520$ nm) at a 1:1 (v/v) ratio. The molar ratio between the number of amine groups of the polymer at a given DNA dose was systematically varied to achieve different N/Ps (1, 2, 3, 5, 10, and 30). The complexes were incubated at r.t. for 20 min to allow stabilization of the formed nanostructures. Subsequently, the samples were diluted 1:16 (v/v) in a 10 mM HEPES buffer solution for fluorescence analysis. Fluorescence measurements (n = 3 per condition) were performed with a Synergy H1 spectrophotometer (BioTek, Italy) in 384-well plates ($\lambda_{ex} = 487$ nm, $\lambda_{em} = 528$ nm). Data are expressed as relative fluorescence normalized to the fluorescence of uncomplexed DNA. The complexation curve of 25 kDa *b*PEI and commercial 10 kDa L-PDMAEMA were used as internal references.

### 2.7. Polyplexes physicochemical characterization

The physicochemical characterization of polyplexes was performed by measuring the size ($D_H$) and surface charge ($\zeta_P$) of the PDMAEMA-based complexes using DLS and ELS analysis using a Malvern Zetasizer Nano ZS instrument. For the analysis, 1 μg of pDNA was complexed in 10 mM HEPES with the different polymer solutions to yield N/P 30. After 20 min incubation at r.t., the samples were transferred to a cuvette containing 650 μL of 10 mM HEPES. The samples were analyzed with a 5 mW HeNe laser, with $\lambda = 633$ nm and a scattering angle of 173°.

### 2.8. In vitro transfection assays

Mycoplasma-free HeLa cells were cultured in Dulbecco's modified Eagle's medium (DMEM) containing 1 mM sodium pyruvate, 10 mM HEPES buffer, 100 U/mL penicillin, 0.1 mg/mL streptomycin, and 2 mM glutamine and supplemented with 10 % (v/v) fetal bovine serum (FBS) (i.e., culture medium) in a humidified atmosphere at 37 °C, under constant supply of 5 % (v/v) $CO_2$.

24 h before transfection assays, cells were plated in 96-well plates at a density of $2 \times 10^4$ cells/cm$^2$ and incubated for 24 h at 37 °C in humidified atmosphere under a constant supply of 5 % $CO_2$ (hereinafter referred to as standard culture conditions). Next, polyplexes were prepared in 10 mM HEPES by mixing polymer solutions with pGL3 (0.25 μg/cm$^2$ dose), to yield complexes at N/P 20, 30, and 40. The resulting complexes were diluted in cDMEM to a final volume of 100 μL/well and then delivered to the cells. Cells were incubated for an additional 24 h under standard culture conditions. Untreated cells were used as negative controls. Cells transfected with 25 kDa *b*PEI/DNA and 10 kDa L-PDMAEMA (i.e., complexes prepared in 10 mM HEPES at N/P 30) were used as the internal reference.

Following a 24 hr-transfection, CT was evaluated using the Alamar Blue® assay, performed according to the manufacturer's protocol. Briefly, the culture medium was replaced with 100 μL of fresh medium containing resazurin solution at a dilution of 1:10 (v/v). Cells were incubated for 2 h under standard culture conditions, then fluorescence was measured using Synergy H1 reader ($\lambda_{ex} = 540$ nm; $\lambda_{em} = 595$ nm). The viability of the negative control (untransfected cells) was set at 100 %, and CT was calculated using the following equation (eq. (2)):

$$cytotoxicity\ (\%) = 100\% - \left(\frac{RFU_{transfected} - RFU_{blank}}{RFU_{control} - RFU_{blank}} \times 100\right) \quad (2)$$

Each term represents the relative fluorescence units (RFU) of transfected samples ($RFU_{transfected}$), blank samples ($RFU_{blank}$), and non-transfected samples ($RFU_{control}$).

TE was evaluated measuring the luciferase activity by means of the Luciferase Assay System according to the manufacturer's instructions. Briefly, cells were washed with PBS and lysed with 110 μL/well of Cell Culture Lysis Reagent diluted 1:20 (v/v) in $dH_2O$. After a freeze-thaw cycle, 20 μL of the lysate was mixed with 50 μL of Luciferase Assay Reagent (diluted 1:2 in PBS). Luminescence was measured using a spectrophotometer. The signal, expressed in relative light units (RLU), was normalized to the protein concentration determined via the BCA assay. TE was reported as RLU/mg of protein.

#### 2.8.1. Chloroquine-mediated transfection

CQ solutions were prepared by diluting CQ at a concentration of 50 mg/mL in $dH_2O$ in the dark. To perform CQ-mediated transfections, HeLa cells were seeded onto separate wells of 96-well plates at a density of $2 \times 10^4$ cells/cm$^2$ and maintained in standard culture conditions for 24 h. Next, polyplexes were prepared as described above (in 2.8) and delivered to cells. After a 6 hr-incubation, 10 μL of CQ solutions were added to each well to reach a final volume of 110 μL yielding a final CQ concentration of 60 μM, then cells were incubated overnight under standard conditions in the dark. Following a 24 hr-transfection, CT and TE were evaluated as described above. Untreated cells (neither polyplexes delivered nor CQ treatment) were used as negative toxicity and transfection controls, while cells challenged with 25 kDa *b*PEI- and 10 kDa L-PDMAEMA-based complexes (N/P 30) in the presence or not of CQ were used as the internal references.

### 2.9. Statistical analysis

Statistical analysis was carried out by GraphPad version 8 (GraphPad software, La Jolla, CA, USA). All data were initially analyzed using D'Agostino and Pearson omnibus normality test. Comparisons among groups were performed by two-way ANOVA (Tukey's multiple comparison test) and multiple *t*-test (Holm-Sidak method). Significance was retained when $p < 0.05$. Data are expressed as mean ± standard deviation (SD). Experiments were performed at least in triplicate.

## 3. Results and discussion

Here, we report the synthesis, physicochemical characterization, and biological evaluation of a structurally diverse library of PDMAEMA-based polymers for non-viral gene delivery. Given the well-established cationic nature of PDMAEMA and its ability to complex NAs, understanding how structural parameters influence TE and biological performance is essential for the rational design of improved gene carriers. Accordingly, the polymers were thoroughly characterized and their biological activity systematically evaluated to correlate structural features with transfection outcomes.

### 3.1. Polymer design and characterization

A library of CPs based on DMAEMA monomeric units was synthesized via ATRP, employing tailored conditions depending on the desired macromolecular topology. Three distinct polymeric structures were obtained by varying the initiator employed in the ATRP process.

Linear $PDMAEMA_m$ (L-$PDMAEMA_m$) homopolymers were synthesized in MeOH using EBiB as the initiator, Cu(I)Br as the catalyst, and BPY as the ligand. Similarly, four-arm $PDMAEMA_m$ (4A- $PDMAEMA_m$) homopolymers were prepared under identical conditions by replacing EBiB with PET-BIB as a tetrafunctional initiator. Amphiphilic block copolymers ($PCL_n$-b-$PDMAEMA_m$) were synthesized in THF using the same catalytic system but with an in-house produced PCL macroinitiator for ATRP ($PCL_n$-Br). This was synthesized via bulk ROP of ε-caprolactone ($\chi_{ROP} \geq 99$ % by $^1$H NMR). The terminal hydroxyl groups of the PCL chains were quantitatively transformed into isobutyryl bromide end groups, yielding well-defined ATRP macroinitiators suitable for the subsequent polymerization of DMAEMA [8,34]. The detailed synthetic pathway followed to obtain the described polymers is reported in Fig. 1A, while a schematic representation of the resulting structures is shown in Fig. 1B.

In the synthesis of the linear polymers, both using the EBIB initiator and the PCL macroinitiator, ATRP of PDMAEMA ensured $\chi_{ATRP} \geq 90$ %,

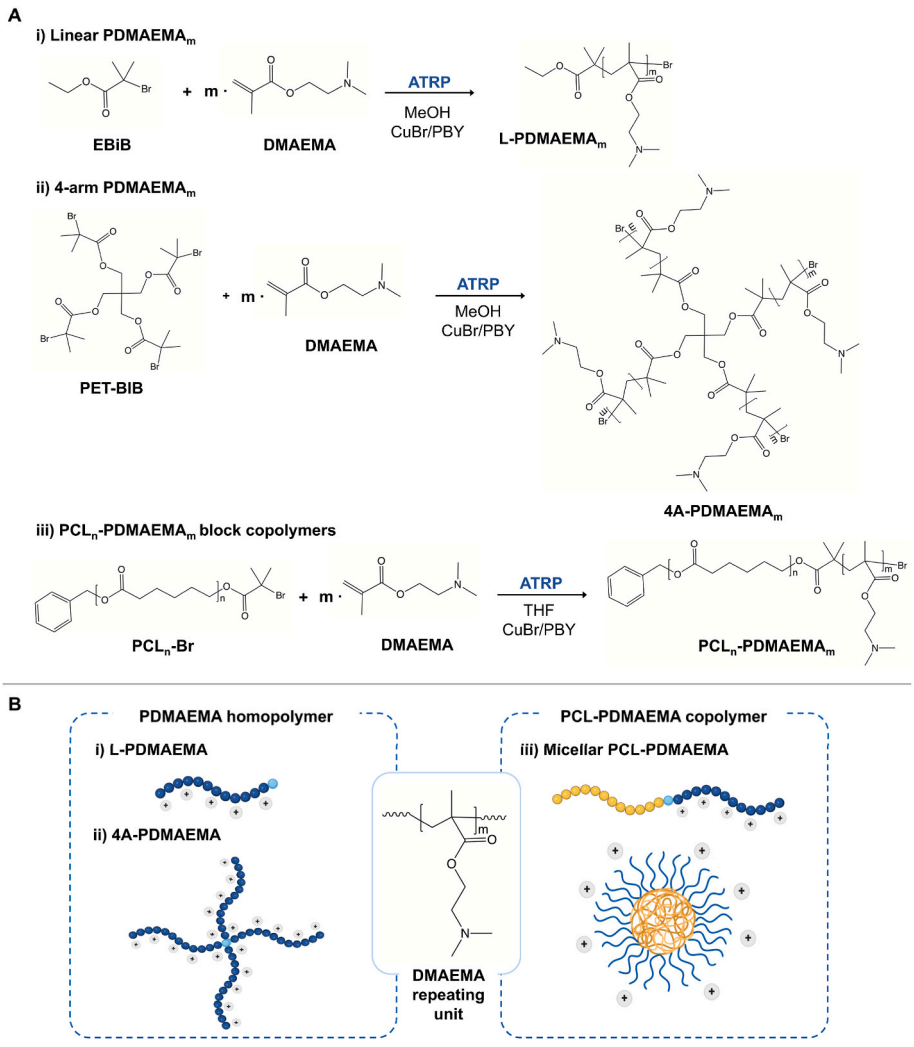


**Fig. 1.** **(A)** Reaction pathways followed for PDMAEMA-based polymers: i) L-PDMAEMA$_m$, ii) 4A-PDMAEMA$_m$, iii) PCL$_n$-b-PDMAEMA$_m$. **(B)** Schematic representation of the resulting structures.

whereas the reaction initiated from the four-arm initiator achieved an average conversion of 85 %. Reaction kinetics were monitored by $^1$H NMR analysis to assess the linearity of the semilogarithmic plots, consistent with first-order behavior, indicating a well-controlled polymerization process (representative profile are reported in Fig. 2A). SEC analysis further confirmed a linear increase of the number-average molar mass ($M_n$) with monomer conversion and a relatively narrow dispersity ($Đ \leq 1.3$), demonstrating the successful synthesis of macromolecules with predictable chain lengths and well-defined topology (Fig. 2B).

To investigate how variations in MW influence polycations CT and TE, L-PDMAEMA$_m$ homopolymers were synthesized with varying chain lengths, corresponding to target DP (m) ranging from 25 to 120 units (MW range going from 4 to 20 kDa).

In parallel, to assess how the incorporation of a hydrophobic segment could alter the physicochemical and biological behavior of the resulting polymers, PCL$_n$-b-PDMAEMA$_m$ was designed comprising 35 units (n) of PCL and 40 units (m) of PDMAEMA. The PDMAEMA block length was

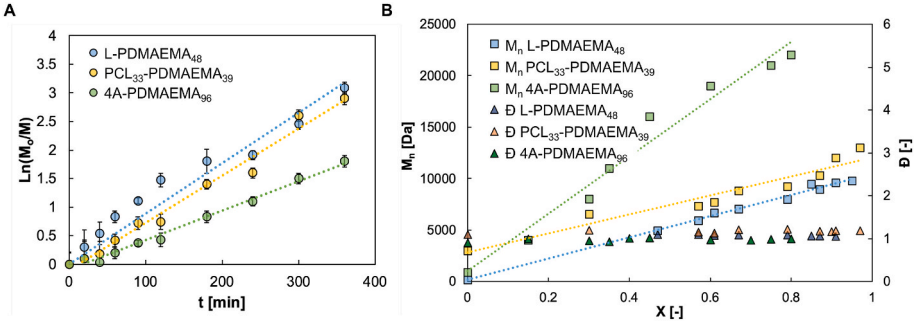


**Fig. 2.** **(A)** Representative polymerization kinetic profiles of L-PDMAEMA$_{48}$, 4A-PDMAEMA$_{96}$, and PCL$_{33}$-PDMAEMA$_{39}$ evaluated via $^1$H NMR. **(B)** Chains growth (expressed as $M_n$) and dispersity (expressed as Đ) as a function of monomer conversion, determined by SEC.

intentionally matched to the homopolymer counterpart having the same number of PDMAEMA monomeric units, enabling a straightforward comparison between the two systems.

To investigate how branched architecture could alter the physicochemical properties and biological performances of PDMAEMA polymers, four-arm homopolymers (4A-PDMAEMA$_m$) with varying MW and arm lengths were synthesized. Three distinct structures were designed to enable systematic comparison with linear counterparts: i) a polymer with a target DP per arm of 120 units, matching the maximum DP targeted in the linear homopolymers series; ii) a polymer with DP of 40 units per arm, enabling direct comparison with both the L-PDMAEMA homopolymer and PCL-b-PDMAEMA copolymer presenting the same number of DMAEMA units; iii) a polymer with target MW of ~15 kDa, enabling comparison with the linear counterpart of equivalent MW. This design enabled a systematic evaluation of the combined effects of MW and arm length on the performance of branched PDMAEMA structures.

The complete list of synthesized polymers and their characterization data are reported in Table 1, while their structures are schematically reported in Fig. 1B. $^1$H NMR spectra and SEC chromatograms for the different polymers are provided in Figs. S1 and S2, respectively.

The protonation behavior of the synthesized polymers was further characterised by potentiometric acid-base titration (Fig. S3). The apparent pKa values, determined by the half-equivalence point method, are reported in Table S1. L-PDMAEMA polymers displayed apparent pKa values in the range 5.5-6.4, while 4A-PDMAEMA polymers exhibited higher pKa values of 6.5-6.6, all falling within a narrow window (≈5.5-6.6) below the physiological pH of 7.4 and overlapping the late-endosomal acidification range (≈6.5 → 5.0). Within the L-PDMAEMA series the apparent pKa increased only slightly with MW (5.5 → 6.4), and these apparent values, as for any polyelectrolyte, are conditional on the low ionic strength of the titration medium. Notably, the 4A-PDMAEMA polymers sat at the upper end of this window (6.5-6.6), comparable to the highest-MW L-PDMAEMA (6.4) rather than markedly higher, consistent with a modestly reduced nearest-neighbour electrostatic penalty per amine in the four-arm architecture [23].

The PCL-PDMAEMA copolymer was evaluated in the form of polymer micelles (M-PCL-PDMAEMA) obtained through a nanoprecipitation process. Such nanostructures were characterized by DLS to assess their size distribution ($D_H$ and PdI), and zeta potential as indirect indicator of the surface charge and colloidal stability ($\zeta_P$) (Fig. S4). The analysis revealed a monomodal population (PdI ≤0.15), with a single peak accounting for 100 % of the scattering intensity, displaying an average $D_H$ of 50 nm and an average $\zeta_P$ of +32 mV.

### 3.2. Evaluation of the DNA complexation ability of PDMAEMAs

For gene delivery applications, a critical prerequisite is the ability of a CP to interact with and effectively condense NAs. PDMAEMA is a water-soluble polymer bearing pendant tertiary amine groups [35]. At physiological pH, a substantial fraction of these amine groups undergoes protonation, thereby enabling electrostatic interactions with the negatively charged phosphate backbone of DNA [36].

To quantify the DNA-binding efficiency of PDMAEMA at various N/Ps, the SYBR Green I exclusion assay was employed. This assay enables determination of the threshold N/P (minimal N/P) ratio required for efficient DNA complexation by monitoring the displacement of the intercalating dye upon polyplex formation. Complexation profiles were obtained by plotting relative fluorescence intensity (expressed as % of uncomplexed DNA) against increasing N/P values.

Comparative complexation profiles were obtained for L-PDMAEMA architectures (Fig. S5 A-H) and 4A-PDMAEMA or micellar (M − ) PCL-PDMAEMA copolymers (Fig. S5 I-L). All synthesized linear polymers were compared with commercial 10 kDa L-PDMAEMA (Fig. S5 M) to evaluate potential MW-dependent differences. Branched polymers were instead benchmarked against 25 kDa *b*PEI (Fig. S5 N) due to their structurally comparable architecture.

As clearly shown in Fig. S5, all polymers displayed characteristic sigmoidal complexation curves, characterized by a steep decline in fluorescence intensity with increasing N/P, indicative of progressive DNA condensation.

For the L-PDMAEMA series, nearly complete DNA complexation was achieved at N/P 3 to 5, exhibiting performance comparable to 25 kDa *b*PEI. Interestingly, minor variations were observed among polymers with different MW, with higher MW polymers (11.0 kDa, 16.5 kDa, and 19.1 kDa) achieving faster fluorescence quenching. This suggests that longer polymer chains facilitate more efficient electrostatic interaction and wrapping around DNA strands with respect to shorter counterparts.

In contrast, the 4-arm and micelle-forming architectures exhibited distinct behavior (Fig. S5 I-L). Although fluorescence intensities decreased sharply at low N/Ps, residual fluorescence of approximately 10-20 % persisted even at high N/Ps for 25.2 kDa 4A-PDMAEMA and 52.3 kDa 4A-PDMAEMA, suggesting incomplete DNA condensation. This behavior points to steric constraints and limited chain mobility within the 4-arm architectures, which may limit accessibility of PDMAEMA segments to the DNA phosphate backbone. However, nearly complete complexation was observed for the 16.5 kDa 4A-PDMAEMA, possibly as a consequence of its lower MW. As for micellar topologies (10.1 kDa M-PCL$_{33}$-PDMAEMA$_{39}$), a similar behavior is found, allowing us to speculate that DNA complexation occurs predominantly at the outer surface of the particle, as cationic units sequestered within the hydrophobic core remain largely inaccessible [36], thus resulting in a superficial "adsorption-like" mechanism rather than intimate inter-polyelectrolyte complexation [37]. As expected, 25 kDa *b*PEI showed its characteristic complexation curve, with complete DNA condensation at N/P 3 [2].

Overall, these data demonstrate that polymer topology and composition significantly influence DNA complexation ability of PDMAEMAs. These findings underscore the importance of balancing polymer

**Table 1**
Structural and molecular characteristics of L-PDMAEMA$_m$, 4A-PDMAEMA$_m$, and PCL$_n$-PDMAEMA$_m$ polymers[a].

| Polymer | Architecture | $m_{TH}$ [−] | m [−] | $M_{n,NMR}$ [kDa] | $M_{n,SEC}$ [kDa] | Đ [−] |
|---|---|---|---|---|---|---|
| L-PDMAEMA$_m$ | Linear | 25 | 23 | 3.9 | 4.2 | 1.1 |
| L-PDMAEMA$_m$ | Linear | 35 | 34 | 5.6 | 6.4 | 1.1 |
| L-PDMAEMA$_m$ | Linear | 40 | 37 | 6.0 | 6.7 | 1.2 |
| L-PDMAEMA$_m$ | Linear | 50 | 48 | 7.8 | 8.2 | 1.1 |
| L-PDMAEMA$_m$ | Linear | 70 | 68 | 11.0 | 12.7 | 1.2 |
| L-PDMAEMA$_m$ | Linear | 110 | 103 | 16.5 | 17.5 | 1.3 |
| L-PDMAEMA$_m$ | Linear | 120 | 120 | 19.1 | 20.1 | 1.2 |
| 4A-PDMAEMA$_m$ | 4-arm | 100 (25 per arm) | 96 (24 per arm) | 16.5 | 17.7 | 1.2 |
| 4A-PDMAEMA$_m$ | 4-arm | 160 (40 per arm) | 156 (39 per arm) | 25.2 | 29.2 | 1.2 |
| 4A-PDMAEMA$_m$ | 4-arm | 480 (120 per arm) | 330 (82 per arm) | 52.3 | 56.5 | 1.2 |
| PCL$_n$-PDMAEMA$_m$ | Di-block | 40 | 39 | 10.1 | 11.1 | 1.2 |

[a] $m_{TH}$ indicates the theoretical degree of polymerization targeted for the DMAEMA ATRP reaction, while $m = \chi_{ATRP} \cdot m_{TH}$ indicates the real PDMAEMA DP based on ATRP conversion ($\chi_{ATRP}$). $M_{n,NMR}$ refers to the number average molecular weight obtained by $^1$H NMR, while $M_{n,SEC}$ and Đ refer to number average molecular weight and chains dispersity obtained by SEC.

architecture in the rational design of PDMAEMA-based gene delivery vectors.

### 3.3. Physicochemical characterization of PDMAEMA-based polyplexes

Understanding how polymer MW and topology govern polyplex formation is essential for rational vector design, as these structural parameters directly influence complex stability, colloidal behavior, and biological performance. In particular, variations in chain length and architecture can modulate DNA condensation efficiency, particle size, surface charge, and ultimately cellular interactions that determine transfection outcomes.

To investigate the influence of polymer topology and MW on polyplexes properties, all formulations were characterized by DLS and ELS to determine their size ($D_H$) and zeta potential ($\zeta_P$), respectively.

All polyplexes were prepared at N/P 30, selected to saturate the electrostatic interactions between PDMAEMA amines and DNA phosphates, thereby providing a consistent basis for inter-formulation comparison independent of the variability arising from sub-saturating ratios. At this ratio complexation is maximal for each polymer, the 4A-PDMAEMA architectures nonetheless retaining a residual uncomplexed fraction owing to steric constraints rather than to an insufficient N/P. For L-PDMAEMA homopolymers, samples were grouped into three MW categories based on their physicochemical behavior: LMW (3.9-7.8 kDa), medium-molecular-weight (MMW, 11–16.5 kDa), and HMW (19.1 kDa). Within each category, $D_H$ and $\zeta_p$ values were averaged to facilitate data interpretation (Fig. 3A–C). Non-linear architectures, including 4A-PDMAEMA variants (16.5, 25.2, and 52.3 kDa) and the micellar 10.1 kDa M-PCL-PDMAEMA were analyzed individually due to their distinct structural features (Fig. 3B–D). Representative size distribution profiles are provided in Fig. S6–S10.

L-PDMAEMA polyplexes exhibited MW-dependent decrease in size, with LMW formulations yielding particles of ≈160 nm, which decreased to 120-130 nm for MMW and HMW polymers (Fig. 3A). This size reduction likely reflects more efficient DNA condensation by longer polymer chains. Conversely, $\zeta_P$ increased with MW, ranging from +10 mV to +20 mV (Fig. 3C), consistent with the higher number of protonable amine groups in larger polymers leading to enhanced surface charge.

The 10 kDa L-PDMAEMA, despite its lower MW, also forms relatively compact polyplexes. This behavior may reflect differences in dispersity, end-group chemistry, or preparation conditions affecting polymer protonation, chain conformation, and self-assembly kinetics. Overall, these observations suggest that polyplex size is not dictated by MW alone, but can also be influenced by subtle variations in polymer structure, handling, and assembly dynamics.

Conversely, 4A-PDMAEMAs polyplexes displayed $D_H$ values ranging from 135 nm to 148 nm, across all MW tested, with no significant MW-dependent increase or decrease in $D_H$ values (Fig. 3B). Similarly, M-PCL-PDMAEMA polyplexes formed particles of ≈125-130 nm (Fig. 3B).

Surface charge measurements revealed no statistically significant differences in $\zeta_P$ among non-linear polymers (Fig. 3D), while all 4A-PDMAEMA variants exhibited statistically significantly lower $\zeta_p$ values compared to 25 kDa *b*PEI, irrespective of MW. This discrepancy likely arises from the distinct three-dimensional architecture of branched polymers, wherein partial sequestration of cationic groups within the polymer framework reduces the net surface charge density accessible for electrostatic stabilization.

For what concerns M-PCL-PDMAEMA, a marked decrease in $\zeta_P$ with respect to 25 kDa *b*PEI further supports our hypothesis that DNA complexation occurs predominantly at the outer surface of the particle because cationic units positioned within the hydrophobic core remain mostly inaccessible, as speculated in the previous paragraph.

### 3.4. Evaluation of cytotoxicity and transfection efficiency under standard conditions

Consistent with the analytical framework described above, CT and TE were evaluated and compared by classifying L-PDMAEMA-based polymers into the previously defined MW categories (LMW, MMW, and HMW). Non-linear architectures (4A-PDMAEMAs and M-PCL-PDMAEMA) were analyzed individually.

Linear polymers displayed strong and consistent MW-dependent increase in TE across all tested N/Ps (Fig. 4B). HMW polymers significantly outperformed LMW and MMW analogs, achieving the highest TE at every tested N/P ($p < 0.05$ vs. LMW and MMW). This superior performance is particularly evident at N/P 30 and 40, where HMW L-PDMAEMA-based polyplexes reached TE values comparable to or exceeding those of the gold standard 25 kDa *b*PEI-based polyplexes ($p > 0.05$).

MMW L-PDMAEMA exhibited intermediate performance, reaching approximately 60 % of *b*PEI polyplexes efficiency, while LMW polymers showed the lowest TE among the synthesized linear series.

Commercial 10 kDa L-PDMAEMA exhibited TE values comparable to those of LMW L-PDMAEMA polyplexes formulations across all tested N/Ps (Fig. 4B), while MMW and HMW L-PDMAEMA performance notably exceeded that of the commercial reference. This difference may reflect differences in purification procedures that affect residual amine protonation in the isolated polymer, consequently altering the effective protonation degree upon pH adjustment prior to formulation.

These results further validate the quality and reproducibility of the in-house synthesis, while also indicating that polymers within this low

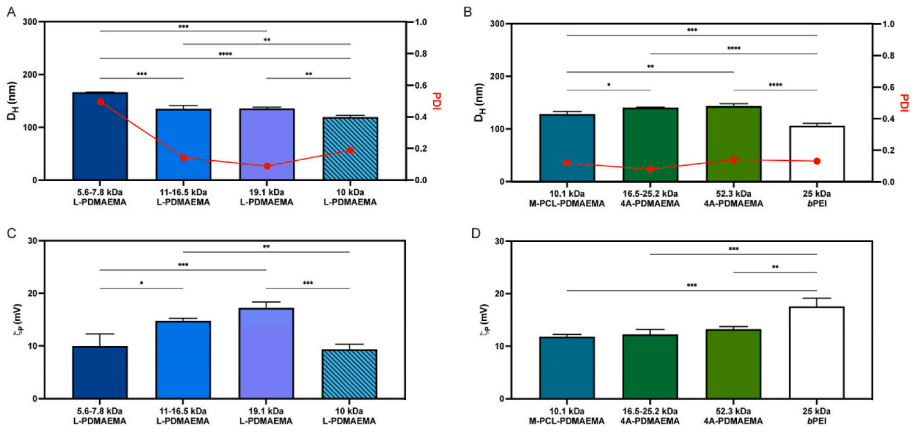


**Fig. 3. Physicochemical characterization of pDNA/PDMAEMA polyplexes**. Results are reported in terms of mean $D_H$ and PdI for: (**A**) L-PDMAEMA grouped according to their MW, (**B**) 4A-PDMAEMA and M-PCL-PDMAEMA. Overall surface charge ($\zeta_P$) is reported for: (**C**) L-PDMAEMA grouped according to their MW and (**D**) 4A-PDMAEMA and M-PCL-PDMAEMA. All polymers were tested at N/P 30. Results are expressed as mean ± SD (n = 3) (*$p < 0.05$; **$p < 0.01$; ****$p < 0.0001$).

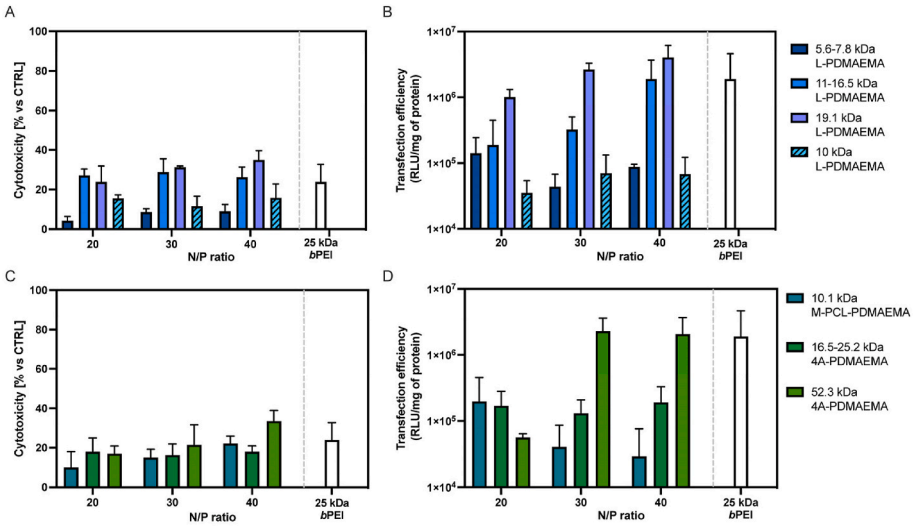


**Fig. 4. CT and TE of PDMAEMA-based complexes in standard conditions**. Graphs show the CT of the sample evaluated after 24 h from transfection for: **(A)** L-PDMAEMA grouped according to their MW, **(C)** 4A-PDMAEMA, and M − PCL-PDMEMA. The TE is expressed as RLU/mg of proteins and results from standard transfections are reported for: **(B)** L-PDMAEMA grouped according to their MW, **(D)** 4A-PDMAEMA, and M − PCL-PDMEMA. Results are expressed as mean ± SD (n = 3). To define the statistical significance, a two-way ANOVA was conducted. Differences are reported in plots as: (*) if $p < 0.05$, (**) if $p < 0.01$, (***) if $p < 0.001$, and not shown when $p > 0.05$ (no statistical significance).

MW regime possess inherently limited transfection capability due to insufficient chain length for efficient NA condensation. This trend is consistent with previous experimental studies demonstrating that PDMAEMA TE increases with MW as a result of stronger DNA binding and improved complex stability, whereas LMW polymers form less compact and less stable polyplexes with reduced biological activity [24,38]. More recent reports on PDMAEMA-based delivery systems similarly confirm that higher MW formulations exhibit enhanced gene expression compared with lower-MW analogs under comparable conditions. Collectively, these observations establish a clear performance hierarchy (HMW > MMW > LMW PDMAEMA) and align with the broader literature indicating the existence of a minimum effective chain length for functional gene delivery, with the present data further suggesting that meaningful improvements in TE require progression to at least the MMW range (16–17 kDa) [39,40].

Importantly, the MW–dependent behavior should be interpreted in light of the associated physicochemical characteristics of the polyplexes. From a SAR perspective, TE appears to correlate primarily with particle size and surface charge rather than MW alone. Complexes formed with HMW L-PDMAEMA tended to exhibit reduced $D_H$ and more positive $\zeta_p$ (Fig. 3A), consistent with more efficient NA condensation and increased surface charge density. Nanoparticles within the sub-200 nm range are generally associated with enhanced endocytic uptake, while higher positive surface charge can strengthen electrostatic interactions with the negatively charged cellular membrane, facilitating internalization [41,42]. Furthermore, the formation of more compact and highly charged complexes is expected to improve NA protection during extracellular exposure and intracellular trafficking [43,44]. Collectively, these size-, charge-, and trafficking-related factors provide a mechanistic basis for the superior TE observed for the HMW systems.

The parallel increase in both CT (Fig. 4A) and TE (Fig. 4B) with increasing MW reflects the dual role of cationic charge density in PDMAEMA-based systems. Longer chains with higher charge density form more compact polyplexes that enhance DNA protection and cellular uptake (thereby improving TE), but simultaneously increase nonspecific electrostatic interactions with cellular membranes (thereby elevating toxicity) [41,45]. The observation that HMW PDMAEMA polyplexes achieve TE comparable to *b*PEI while maintaining similar CT demonstrates that these polymers represent an optimal balance between efficacy and biocompatibility.

Notably, these results indicate that effective gene delivery can be achieved with polymer MWs considerably below those employed in many earlier studies [40], provided that formulation pH is carefully controlled during polyplex assembly. Precise pH adjustment to physiological conditions ensures optimal protonation of PDMAEMA amine groups, maximizing DNA condensation efficiency and polyplex stability. This finding underscores that polymer handling and formulation protocols are as critical as intrinsic structural parameters in determining biological performance.

The CT and TE of polyplexes obtained with polymer displaying complex topologies are reported in Fig. 4C–D. Non-linear architectures exhibited TE behavior characterized by progressive increases as a function of N/P (Fig. 4D). Within the 4A-PDMAEMA series, TE increased substantially from N/P 20 to N/P 40 for all formulations tested. Notably, the 52.3 kDa 4A-PDMAEMA (which represents the 4-arm topological analog of the 19.1 kDa HMW linear polymer in terms of PDMAEMA content per chain) achieved TE values at N/P 30-40 that were comparable to those of both its linear counterpart (19.1 kDa L-PDMAEMA, Fig. 4B) and the gold-standard 25 kDa *b*PEI.

The lower MW star polymers (16.5 and 25.2 kDa 4A-PDMAEMA) displayed similar N/P-dependent trends. These formulations achieved TE values at N/P 30-40 that were comparable to or slightly lower than those of the 52.3 kDa variant. This behavior likely reflects reduced charge accessibility arising from steric hindrance within the branched topology. The 4-arm architecture inherently limits the conformational flexibility of individual PDMAEMA segments, likely reducing their ability to efficiently wrap around and condense DNA molecules. Additionally, steric crowding at the branching points may hinder optimal alignment of cationic groups with the DNA phosphate backbone, resulting in less compact and less stable polyplexes compared to their linear analogs. This interpretation is consistent with the physicochemical data presented in Fig. 3D, where 16.5-25.2 kDa and 52.3 kDa 4A-PDMAEMA exhibited lower surface charge density (slightly higher than +10 mV) compared to the linear formulations of equivalent MW (~+15-20 mV), i.e., 11-16.5 kDa and 19.1 kDa L-PDMAEMA, respectively, thus reflecting suboptimal DNA condensation. Within the 4A-PDMAEMA series, polyplex CT showed minimal MW-dependence, with all formulations exhibiting comparable values regardless of chain length (Fig. 4C).

The micellar structure consistently exhibited the lowest TE values

across all N/Ps. However, this architecture was not further explored, as micellar conformations are presumed to demand a more comprehensive investigation of the hydrophilic-hydrophobic balance to fully optimize their performance.

Direct comparison of topological analogs (52.3 kDa 4A-PDMAEMA vs. 19.1 kDa L-PDMAEMA), both containing approximately the same number of DMAEMA repeating units per chain, revealed no significant differences in TE ($p > 0.05$) across the N/P range tested, with both formulations reaching approximately $5 \times 10^6$ RLU/mg of protein at N/P 30-40. This observation suggests that, under the conditions tested, polymer topology and the number of arms/chains do not exert a dominant influence on TE. Instead, the data indicate that MW, or more precisely, the total number of cationic DMAEMA units available for DNA complexation, is the primary structural determinant of TE across both linear and branched architectures. Similarly, no significant differences in toxicity were observed across the N/P range tested. The PDMAEMA formulation at N/P 30 therefore represents an optimized structure within this polymer library, matching the performance of both HMW L-PDMAEMA and 25 kDa *b*PEI while providing superior biocompatibility.

However, despite these encouraging results, the overall transfection levels only approach those typically achieved with more efficient vectors, suggesting that intracellular barriers, particularly limited endosomal escape capacity, may represent a key bottleneck for PDMAEMA-based systems improvement. Although PDMAEMA possesses buffering amine groups that can contribute to a proton sponge effect, its buffering capacity and membrane-disruptive activity are generally lower than those of more effective polymers such as *b*PEI, potentially resulting in inefficient endosomal destabilization and lysosomal degradation of internalized polyplexes. This limitation indicates that strategies specifically aimed at enhancing endosomal escape, such as increasing buffering density, incorporating membrane-active or pH-responsive functionalities, or promoting endosomal membrane destabilization, may be required to further improve the intracellular delivery efficiency and overall transfection performance of PDMAEMA-based vectors.

### 3.5. Investigation of endosomal escape efficiency through chloroquine-mediated enhancement

While the SAR study established MW as the dominant structural parameter governing TE in PDMAEMA-based systems, the mechanistic basis for this MW-dependent performance remains incompletely understood. This requires identifying which intracellular barrier is most critically influenced by polymer structure. Among these, endosomal escape represents a particularly critical bottleneck for PDMAEMA-based systems as they exhibit limited intrinsic capability to disrupt endosomal membranes [46], and this issue may differentially impact polymers of varying MW and topology. We therefore hypothesized that endosomal entrapment may be a major factor limiting TE in PDMAEMA formulations, and that this barrier may be variably impacted by variations in polymer MW and topology.

To test this hypothesis, we employed CQ as a chemical probe to selectively relieve the endosomal escape constraint. CQ disrupts endosomal membranes through pH buffering and osmotic swelling [26,28], effectively bypassing the polymer's intrinsic endosomal release mechanism. By comparing transfection performance with and without CQ treatment, we could directly assess the extent to which endosomal entrapment limits each formulation.

All experiments were conducted at N/P 30, providing a standardized condition with sufficient measured TE to clearly detect CQ-induced enhancements across the entire polymer library.

As clearly shown in Fig. 5, CQ treatment produced markedly different effects depending on polymer structure. Specifically, L-PDMAEMA-based polyplexes exhibited dramatic responsiveness across all MW categories (Fig. 5B), with LMW and MMW showing ~20-fold increases in TE, while HMW L-PDMAEMA achieved up to 30-fold enhancement (Fig. 6A).

Across all tested conditions, CT remained within acceptable limits and did not reach levels typically associated with severe cellular stress (Fig. 5A). Overall, the CT profiles were comparable among the different L-PDMAEMA formulations, regardless of polymer MW or topology. The inclusion of CQ did not significantly impact cell viability, indicating that its endosomal-disruptive effect did not exacerbate membrane damage or induce additional cytotoxic responses.

In striking contrast, 4A-PDMAEMA architectures exhibited minimal CQ-responsiveness (Fig. 5D), demonstrating negligible enhancement (Fig. 6B). This behavior is consistent with that of 25 kDa *b*PEI, which also showed no TE improvement upon CQ treatment. This observation likely reflects the fact that *b*PEI already possesses comparatively

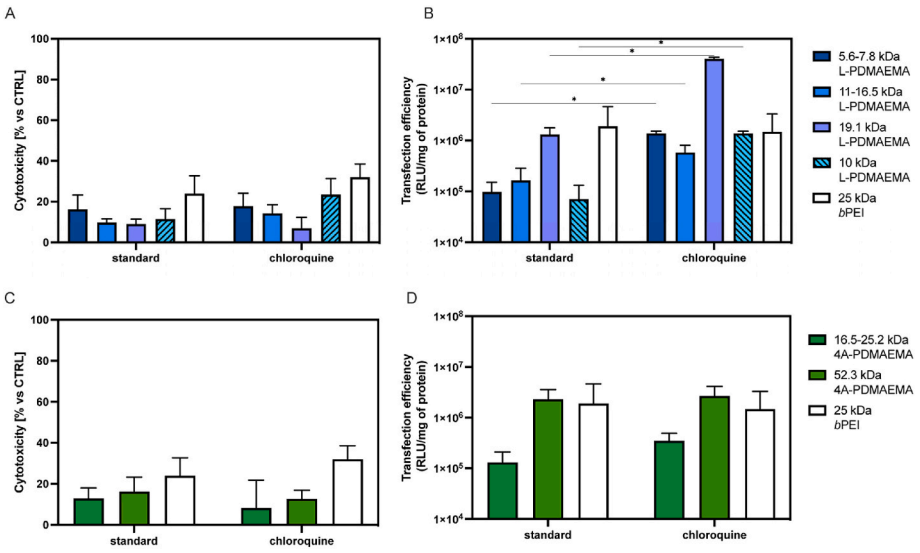


**Fig. 5. CT and TE of PDMAEMA-based complexes in CQ-mediated transfections conditions at N/P 30.** Graphs show the CT of the sample evaluated after 24 h from transfection in CQ-mediated conditions for: (**A**) L-PDMAEMA grouped according to their MW, (**C**) 4A-PDMAEMA, and M-PCL-PDMAEMA. TE is expressed as RLU/mg of proteins. Results from CQ-mediated transfections are reported for: (**B**) L-PDMAEMA grouped according to their MW, (**D**) 4A-PDMAEMA, and M-PCL-PDMAEMA. Results are expressed as mean ± SD (n = 3). To define the statistical significance, a *t*-test was conducted. Differences are reported in plots as: (*) if $p < 0.05$, (**) if $p < 0.01$, (***) if $p < 0.001$, and not shown when $p > 0.05$ (no statistical significance).

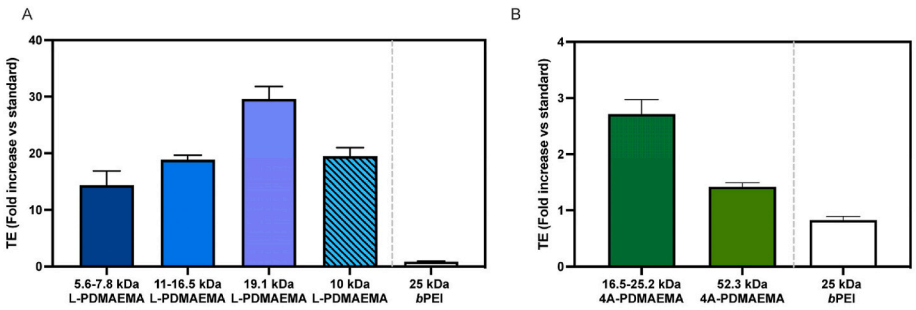


**Fig. 6.** Fold increase in TE for cells treated with CQ with respect to standard transfections are reported for (**A**) L-PDMAEMA and (**B**) 4A/M-PDMAEMA. Results are expressed as mean ± SD (n = 3).

efficient endosomal escape capability [47], such that pharmacological augmentation through CQ provides no additional benefit. The minimal CQ-responsiveness of 4A-PDMAEMA suggests that endosomal escape is not the primary rate-limiting barrier for branched architectures. Rather, alternative bottlenecks, such as reduced cellular uptake (consistent with the larger, lower-charged polyplexes observed in Fig. 3B–D), likely constrain 4A-PDMAEMA performance, meaning that enhanced endosomal release alone is insufficient to improve transfection.

This mechanistic dichotomy is further supported by the calculated pKa values. For L-PDMAEMA, the apparent pKa confirms proton uptake during endosomal acidification; however, this buffering is insufficient for autonomous membrane rupture, consistent with PDMAEMA inducing membrane strain rather than lysis [46]. The comparable CQ-induced increase in TE across the entire L-PDMAEMA MW range indicates that polyplexes reach the endosomes but remain trapped there. The 4A-PDMAEMA polymers display a comparable apparent pKa, and therefore comparable endosomal buffering, yet show negligible CQ enhancement. This confirms that endosomal escape is not the rate-limiting step for these polymers and that their lower TE instead reflects the upstream uptake bottleneck noted above, rather than impaired endosomal escape.

Overall, these observations underscore that polymers that suffer from severe endosomal escape deficiency show dramatic TE enhancement upon CQ addition, whereas CQ-unresponsive formulations either possess adequate intrinsic escape capability (as in the case of *b*PEI) or face alternative rate-limiting barriers (as observed for 4A-PDMAEMA). These findings have direct implications for rational vector design. Further optimization of L-PDMAEMA requires addressing endosomal escape through chemical modification (e.g., incorporation of fusogenic peptides or pH-sensitive moieties) or co-treatment strategies, whereas improving branched variants necessitates enhancing cellular uptake or facilitating intracellular unpacking-interventions unrelated to endosomal release mechanisms.

## 4. Conclusions

This study provides a systematic SAR analysis of PDMAEMA-based polymers as non-viral gene delivery vectors, establishing how MW, architecture, and endosomal escape capability collectively govern transfection performance and CT.

Polyplexes made of L-PDMAEMA polymers with higher MW (19.1 kDa) achieved TE comparable to the gold standard 25 kDa *b*PEI counterparts, while maintaining acceptable cytoxicity profiles.

Comparative analysis of topological analogs (52.3 kDa 4A-PDMAEMA vs. 19.1 kDa L-PDMAEMA) revealed that polymer architecture exerts minimal influence on both TE and CT when total DMAEMA content is held constant. These findings establish that MW, rather than topology, is the primary determinant of biological performance for PDMAEMA homopolymers.

Potentiometric titration showed that all polymers possess apparent pKa values within a narrow window (≈5.5-6.6), with only modest, MW-independent differences across architectures, the four-arm polymers being comparable to the highest-MW linear analogue rather than markedly higher. These modest differences do not parallel the marked TE differences, establishing that the MW-dependent TE trends cannot be attributed to differences in protonation equilibrium, but instead arise from structural factors governing polyplex formation, stability, and cellular interactions. Taken together, the data point to two distinct optimization routes: improving endosomal escape for L-PDMAEMA (e.g., by incorporating co-monomers that buffer within the 5.5-6.5 window, or membrane-disruptive motifs), and improving cellular uptake for 4A-PDMAEMA (e.g., by introducing targeting ligands).

CQ-mediated experiments provided critical mechanistic insight into performance limitations. Linear PDMAEMA exhibited dramatic CQ-responsiveness (30-fold TE enhancement without increased CT), demonstrating that inefficient endosomal escape represents the dominant barrier constraining these formulations. Importantly, this limitation is MW-independent: all linear polymers showed similarly strong CQ-response, indicating that endosomal entrapment is a pervasive and structure-intrinsic deficiency of L-PDMAEMA that is not substantially addressed by increasing chain length. Thus, the MW-dependent differences observed under basal conditions cannot be attributed to improved intrinsic endosomal escape capability at higher MW, but instead likely arise from upstream factors such as enhanced cellular uptake, polyplex stability, or intracellular trafficking efficiency that increase the number of complexes reaching the endosomal compartment without improving their probability of cytosolic release.

In contrast, branched 4A-PDMAEMA architectures showed minimal CQ-responsiveness, revealing that these formulations face alternative rate-limiting barriers (likely reduced cellular uptake or impaired intracellular unpacking) unrelated to endosomal entrapment. This fundamental mechanistic difference between linear and branched polymers indicates that topology dictates which intracellular barrier becomes rate-limiting.

Overall, this work establishes that optimized PDMAEMA design, formulated under controlled pH conditions, can achieve non-viral gene delivery performance approaching that of *b*PEI while maintaining acceptable toxicity. However, the dramatic TE enhancements obtained through CQ co-treatment reveal that current PDMAEMA formulations operate far below their theoretical potential due to inefficient endosomal escape.

These results provide a foundation for future optimization of PDMAEMA-based gene delivery systems, indicating that 10-20 kDa L-PDMAEMA polymers represent the most promising candidates for further development, particularly if endosomal escape functionality can be intrinsically encoded into the polymer design.

Future work could focus on redesigning M-to-HMW L-PDMAEMA polymers by incorporating monomeric units capable of mimicking CQ's buffering and endosomal escape functions. Such an approach would intrinsically encode this functionality within the polymer backbone, eliminating the need for separate treatments or post-transfection supplementation with external agents. In particular, a deeper

understanding of the precise mechanism of action of CQ may guide the rational development or selection of alternative endosomal escape agents to more effectively facilitate this process. In parallel, systematic variation of the PCL block length in amphiphilic PDMAEMA-based copolymers would provide further insight into the role of hydrophobic content in governing self-assembly, polyplex surface accessibility, and membrane interaction, representing a complementary direction for future investigation.

## CRediT authorship contribution statement

**Flaminia Fruzzetti:** Data curation, Formal analysis, Investigation, Visualization, Writing – original draft, Writing – review & editing. **Ilaria Porello:** Data curation, Investigation, Visualization, Writing – original draft, Writing – review & editing. **Nina Bono:** Conceptualization, Data curation, Formal analysis, Methodology, Supervision, Writing – original draft, Writing – review & editing. **Francesco Cellesi:** Conceptualization, Funding acquisition, Methodology, Project administration, Resources, Supervision, Writing – review & editing. **Gabriele Candiani:** Conceptualization, Funding acquisition, Methodology, Project administration, Resources, Supervision, Writing – review & editing.

## Declaration of competing interest

The authors declare that they have no known competing financial interests or personal relationships that could have appeared to influence the work reported in this paper.

## Acknowledgements

We would like to thank Politecnico di Milano for financial support.

## Appendix A. Supplementary data

Supplementary data to this article can be found online at https://doi.org/10.1016/j.jddst.2026.108613.

## Data availability

Data will be made available on request.

## References

[1] I. Porello, N. Bono, G. Candiani, F. Cellesi, Advancing nucleic acid delivery through cationic polymer design: non-cationic building blocks from the toolbox, Polym. Chem. 15 (2024) 2800–2826, https://doi.org/10.1039/D4PY00234B.
[2] N. Bono, F. Ponti, D. Mantovani, G. Candiani, Non-viral in vitro gene delivery: it is now time to set the bar, Pharmaceutics 12 (2020) 183, https://doi.org/10.3390/pharmaceutics12020183.
[3] D. Pezzoli, G. Candiani, Non-viral gene delivery strategies for gene therapy: a "ménage à trois" among nucleic acids, materials, and the biological environment, J. Nanoparticle Res. 15 (2013) 1523, https://doi.org/10.1007/s11051-013-1523-7.
[4] X. Du, J. Wang, Q. Zhou, L. Zhang, S. Wang, Z. Zhang, C. Yao, Advanced physical techniques for gene delivery based on membrane perforation, Drug Deliv. 25 (2018) 1516–1525, https://doi.org/10.1080/10717544.2018.1480674.
[5] A.J. Mellott, M.L. Forrest, M.S. Detamore, Physical non-viral gene delivery methods for tissue engineering, Ann. Biomed. Eng. 41 (2013) 446–468, https://doi.org/10.1007/s10439-012-0678-1.
[6] J.T. Bulcha, Y. Wang, H. Ma, P.W.L. Tai, G. Gao, Viral vector platforms within the gene therapy landscape, Signal Transduct. Targeted Ther. 6 (2021) 1–24, https://doi.org/10.1038/s41392-021-00487-6.
[7] Y. Liu, J. Rohrs, P. Wang, Development and challenges of nanovectors in gene therapy, Nano Life 4 (2014) 1441007, https://doi.org/10.1142/S1793984414410074.
[8] I. Porello, F. Stucchi, G. Sbaruffati, F. Cellesi, Tailoring copolymer architectures and macromolecular interactions for enhanced nanotherapeutic delivery: a design-by-architecture approach, Eur. Polym. J. 220 (2024) 113455, https://doi.org/10.1016/j.eurpolymj.2024.113455.
[9] I.M.S. Degors, C. Wang, Z.U. Rehman, I.S. Zuhorn, Carriers break barriers in drug delivery: endocytosis and endosomal escape of gene delivery vectors, Acc. Chem. Res. 52 (2019) 1750–1760, https://doi.org/10.1021/acs.accounts.9b00177.
[10] C. Qiu, F. Xia, J. Zhang, Q. Shi, Y. Meng, C. Wang, H. Pang, L. Gu, C. Xu, Q. Guo, J. Wang, Advanced strategies for overcoming Endosomal/Lysosomal barrier in Nanodrug delivery, Research 6 (2023), https://doi.org/10.34133/research.0148.
[11] L.M.P. Vermeulen, S.C. De Smedt, K. Remaut, K. Braeckmans, The proton sponge hypothesis: fable or fact? Eur. J. Pharm. Biopharm. 129 (2018) 184–190, https://doi.org/10.1016/j.ejpb.2018.05.034.
[12] Q. Zhang, G. Kuang, W. Li, J. Wang, H. Ren, Y. Zhao, Stimuli-responsive gene delivery nanocarriers for cancer therapy, Nano-Micro Lett. 15 (2023) 44, https://doi.org/10.1007/s40820-023-01018-4.
[13] H. Hatakeyama, E. Ito, H. Akita, M. Oishi, Y. Nagasaki, S. Futaki, H. Harashima, A pH-sensitive fusogenic peptide facilitates endosomal escape and greatly enhances the gene silencing of siRNA-containing nanoparticles in vitro and in vivo, J. Contr. Release 139 (2009) 127–132, https://doi.org/10.1016/j.jconrel.2009.06.008.
[14] J. Chen, J. Li, J. Zhou, Z. Lin, F. Cavalieri, E. Czuba-Wojnilowicz, Y. Hu, A. Glab, Y. Ju, J.J. Richardson, F. Caruso, Metal–phenolic coatings as a platform to trigger endosomal escape of nanoparticles, ACS Nano 13 (2019) 11653–11664, https://doi.org/10.1021/acsnano.9b05521.
[15] F. Ponti, M. Campolungo, C. Melchiori, N. Bono, G. Candiani, Cationic lipids for gene delivery: many players, one goal, Chem. Phys. Lipids 235 (2021) 105032, https://doi.org/10.1016/j.chemphyslip.2020.105032.
[16] Z. ur Rehman, D. Hoekstra, I.S. Zuhorn, Mechanism of Polyplex- and Lipoplex-mediated delivery of nucleic acids: real-time visualization of transient membrane destabilization without endosomal lysis, ACS Nano 7 (2013) 3767–3777, https://doi.org/10.1021/nn3049494.
[17] M.A. Mintzer, E.E. Simanek, Nonviral vectors for gene delivery, Chem. Rev. 109 (2009) 259–302, https://doi.org/10.1021/cr800409e.
[18] P. van de Wetering, E.E. Moret, N.M.E. Schuurmans-Nieuwenbroek, M.J. van Steenbergen, W.E. Hennink, Structure−Activity relationships of water-soluble cationic Methacrylate/Methacrylamide polymers for nonviral gene delivery, Bioconjug. Chem. 10 (1999) 589–597, https://doi.org/10.1021/bc980148w.
[19] P. van de Wetering, J.-Y. Cherng, H. Talsma, W.E. Hennink, Relation between transfection efficiency and cytotoxicity of poly(2-(dimethylamino)ethyl methacrylate)/plasmid complexes, J. Contr. Release 49 (1997) 59–69, https://doi.org/10.1016/S0168-3659(97)00059-X.
[20] M.R. Telaretti Leggieri, T. Kaldéus, M. Johansson, E. Malmström, PDMAEMA from α to ω chain ends: tools for elucidating the structure of poly(2-(dimethylamino) ethyl methacrylate), Polym. Chem. 14 (2023) 1241–1253, https://doi.org/10.1039/D2PY01604D.
[21] W. Jiang, L. Lu, Y. Cai, Highly efficient and well-controlled ambient temperature RAFT polymerization under solar radiation, Macromol. Rapid Commun. 28 (2007) 725–728, https://doi.org/10.1002/marc.200600788.
[22] S. Agarwal, Y. Zhang, S. Maji, A. Greiner, PDMAEMA based gene delivery materials, Mater. Today 15 (2012) 388–393, https://doi.org/10.1016/S1369-7021(12)70165-7.
[23] A. Schallon, V. Jérôme, A. Walther, C.V. Synatschke, A.H.E. Müller, R. Freitag, Performance of three PDMAEMA-based polycation architectures as gene delivery agents in comparison to linear and branched PEI, React. Funct. Polym. 70 (2010) 1–10, https://doi.org/10.1016/j.reactfunctpolym.2009.09.006.
[24] C.V. Synatschke, A. Schallon, V. Jérôme, R. Freitag, A.H.E. Müller, Influence of polymer architecture and molecular weight of Poly(2-(dimethylamino)ethyl methacrylate) polycations on transfection efficiency and cell viability in gene delivery, Biomacromolecules 12 (2011) 4247–4255, https://doi.org/10.1021/bm201111d.
[25] V. Jérôme, C.V. Synatschke, R. Freitag, Transient destabilization of biological membranes contributes to the superior performance of star-shaped PDMAEMA in delivering pDNA, ACS Omega 5 (2020) 26640–26654, https://doi.org/10.1021/acsomega.0c03367.
[26] E. Pandey, E.N. Harris, Chloroquine and cytosolic galectins affect endosomal escape of antisense oligonucleotides after Stabilin-mediated endocytosis, Mol. Ther. Nucleic Acids 33 (2023) 430–443, https://doi.org/10.1016/j.omtn.2023.07.019.
[27] B. Ruzzante, F. Fruzzetti, M. Cattaneo, G. Lauria Pinter, S. Marcuzzo, G. Candiani, N. Bono, Harnessing osmotic shock for enhanced intracellular delivery of (nano) cargos, Int. J. Pharm. 669 (2025) 125008, https://doi.org/10.1016/j.ijpharm.2024.125008.
[28] M. Hajimolaali, H. Mohammadian, A. Torabi, A. Shirini, M. Khalife Shal, H. Barazandeh Nezhad, S. Iranpour, R. Baradaran Eftekhari, F. Dorkoosh, Application of chloroquine as an endosomal escape enhancing agent: new frontiers for an old drug, Expert Opin. Drug Deliv. 18 (2021) 877–889, https://doi.org/10.1080/17425247.2021.1873272.
[29] S.R. Bhattarai, E. Muthuswamy, A. Wani, M. Brichacek, A.L. Castañeda, S.L. Brock, D. Oupicky, Enhanced gene and siRNA delivery by polycation-modified mesoporous Silica nanoparticles loaded with chloroquine, Pharm. Res. 27 (2010) 2556–2568, https://doi.org/10.1007/s11095-010-0245-0.
[30] J. Wang, X. Zhou, H. Wang, Q. Xiao, K. Ding, X. Dong, S. Xu, B. Shen, J. Sun, Z. Zhou, J. Tang, X. Liu, Y. Shen, Autophagy-inhibiting polymer as an effective nonviral cancer gene therapy vector with inherent apoptosis-sensitizing ability, Biomaterials 255 (2020) 120156, https://doi.org/10.1016/j.biomaterials.2020.120156.
[31] L. Flebus, F. Lombart, C. Sevrin, J.-O. Defraigne, P. Peters, L. Parhamifar, D.G. M. Molin, C. Grandfils, Low molecular weight poly (2-dimethylamino ethylmethacrylate) polymers with controlled positioned fluorescent labeling: synthesis, characterization and in vitro interaction with human endothelial cells, Int. J. Pharm. 478 (2015) 278–287, https://doi.org/10.1016/j.ijpharm.2014.11.016.

[32] C.-W. Lo, Y. Chang, J.-L. Lee, W.-B. Tsai, W.-S. Chen, Tertiary-amine functionalized polyplexes enhanced cellular uptake and prolonged gene expression, PLoS One 9 (2014) e97627, https://doi.org/10.1371/journal.pone.0097627.
[33] J. Reijenga, A. van Hoof, A. van Loon, B. Teunissen, Development of methods for the determination of pKa values, J. Drug Deliv. Sci. Technol. 23 (2013) 401–407, https://doi.org/10.4137/ACI.S12304.
[34] I. Porello, F. Stucchi, R. Guarini, G. Sbaruffati, F. Cellesi, TCEP-enabled click modification of Glycidyl-bearing polymers with biorelevant Sulfhydryl molecules: toward chemoselective bioconjugation strategies, Biomacromolecules 26 (2025) 5269–5286, https://doi.org/10.1021/acs.biomac.5c00766.
[35] G.A. Titaux, A. Contreras-García, E. Bucio, Surface modification by γ-ray-induced grafting of PDMAEMA/PEGMEMA onto PE films, Radiat. Phys. Chem. 78 (2009) 485–488, https://doi.org/10.1016/j.radphyschem.2009.03.031.
[36] P. van de Wetering, J.-Y. Cherng, H. Talsma, D.J.A. Crommelin, W.E. Hennink, 2-(dimethylamino)ethyl methacrylate based (co)polymers as gene transfer agents, J. Contr. Release 53 (1998) 145–153, https://doi.org/10.1016/S0168-3659(97)00248-4.
[37] M. Zheng, G.M. Pavan, M. Neeb, A.K. Schaper, A. Danani, G. Klebe, O.M. Merkel, T. Kissel, Targeting the blind spot of polycationic nanocarrier-based siRNA delivery, ACS Nano 6 (2012) 9447–9454, https://doi.org/10.1021/nn301966r.
[38] J. Dou, S. Yu, Y. Zhang, A facile and scalable method to synthesize <scp>PEGylated PDMAEMA</scp> for gene delivery, Biopolymers 115 (2024), https://doi.org/10.1002/bip.23584.
[39] X. Cai, R. Dou, C. Guo, J. Tang, X. Li, J. Chen, J. Zhang, Cationic polymers as transfection reagents for nucleic acid delivery, Pharmaceutics 15 (2023) 1502, https://doi.org/10.3390/pharmaceutics15051502.
[40] J.M. Layman, S.M. Ramirez, M.D. Green, T.E. Long, Influence of polycation molecular weight on Poly(2-dimethylaminoethyl methacrylate)-mediated DNA delivery in vitro, Biomacromolecules 10 (2009) 1244–1252, https://doi.org/10.1021/bm9000124.
[41] E. Fröhlich, The role of surface charge in cellular uptake and cytotoxicity of medical nanoparticles, Int. J. Nanomed. 5577 (2012), https://doi.org/10.2147/IJN.S36111.
[42] Z.-G. Yue, W. Wei, P.-P. Lv, H. Yue, L.-Y. Wang, Z.-G. Su, G.-H. Ma, Surface charge affects cellular uptake and intracellular trafficking of chitosan-based nanoparticles, Biomacromolecules 12 (2011) 2440–2446, https://doi.org/10.1021/bm101482r.
[43] S.E.A. Gratton, P.A. Ropp, P.D. Pohlhaus, J.C. Luft, V.J. Madden, M.E. Napier, J. M. DeSimone, The effect of particle design on cellular internalization pathways, Proc. Natl. Acad. Sci. 105 (2008) 11613–11618, https://doi.org/10.1073/pnas.0801763105.
[44] J. Rejman, V. Oberle, I.S. Zuhorn, D. Hoekstra, Size-dependent internalization of particles via the pathways of clathrin- and caveolae-mediated endocytosis, Biochem. J. 377 (2004) 159–169, https://doi.org/10.1042/bj20031253.
[45] S.T. Kim, K. Saha, C. Kim, V.M. Rotello, The role of surface functionality in determining nanoparticle cytotoxicity, Acc. Chem. Res. 46 (2013) 681–691, https://doi.org/10.1021/ar3000647.
[46] R.A. Jones, M.H. Poniris, M.R. Wilson, pDMAEMA is internalised by endocytosis but does not physically disrupt endosomes, J. Contr. Release 96 (2004) 379–391, https://doi.org/10.1016/j.jconrel.2004.02.011.
[47] O. Boussif, F. Lezoualc'h, M.A. Zanta, M.D. Mergny, D. Scherman, B. Demeneix, J. P. Behr, A versatile vector for gene and oligonucleotide transfer into cells in culture and in vivo: polyethylenimine, Proc. Natl. Acad. Sci. U. S. A. 92 (16) (1995 Aug 1) 7297–7301. https://www.pnas.org/doi/abs/10.1073/pnas.92.16.7297.